

Beam gas curtain monitor: Vacuum studies for LHC integration and operation

C. Castro Sequeiro¹,* M. Ady¹, G. Bregliozzi, N. Chatzigeorgiou, A. R. Churchman,
R. Kersevan¹, T. Lefevre¹, S. Mazzoni¹, G. Pigny, A. Rossi¹, M. Sameed¹, G. Schneider¹,
O. Sedlacek¹, K. Sidorowski¹, C. Vazquez Pelaez¹, R. Veness¹, and L. Zygaropoulos¹

CERN, European Organization for Nuclear Research, 1211 Meyrin, Switzerland

O. Stringer², A. Webber-Date, C. P. Welsch², and H. Zhang²

University of Liverpool/Cockcroft Institute, WA4 4AD Warrington, United Kingdom

P. Forck³ and S. Udrea³

GSI, 64291 Darmstadt, Germany



(Received 11 October 2023; accepted 7 March 2024; published 12 April 2024)

A beam gas curtain (BGC) monitor has been designed to obtain information about the relative position between the LHC proton beam and the hollow electron lens electron beam through a minimally invasive process. Its working principle relies on intersecting the path of both beams with a supersonic gas curtain, introduced transversely into the LHC beamline, to produce a fluorescence signal. As an intermediate project stage (phase II), a preliminary version of the BGC monitor has been installed into the LHC beamline. To ensure the successful integration of the monitor and subsequent operation under LHC ultrahigh vacuum conditions, a series of vacuum studies have been performed. These can be classified as follows: An off-line laboratory test campaign, to assess BGC behavior during pump down and gas injections; simulations and analytical calculations, to evaluate BGC behavior and estimate the impact of its installation and operation in the LHC. This document will briefly present the off-line tests campaign, followed by a more extensive description of the simulations performed.

DOI: [10.1103/PhysRevAccelBeams.27.043201](https://doi.org/10.1103/PhysRevAccelBeams.27.043201)

I. INTRODUCTION

Within the Hi-Lumi LHC upgrade, a beam gas curtain (BGC) monitor has been developed to be part of the hollow electron lens (HEL), a device dedicated to control halo particles [1]. The objective of the BGC monitor is to obtain information about the relative position of the LHC proton beam in the hollow electron beam created at the HEL, producing the highest possible signal while having minimum impact on the beams and vacuum conditions. To do so, a thin gas curtain is generated at the monitor and introduced into the LHC beamline, intersecting both beams. Fluorescence is thus produced from the interactions between particles and captured by an optical system [2–4]. Beam monitors with similar working principles have been developed in parallel around the world [5–7].

The curtain is generated at the BGC by letting gas at high pressure (5 bar) to expand through a 30 μm diameter nozzle into the so-called injection chamber. Then the gas passes through three different skimmers that give it the adequate shape and density before reaching the interaction chamber. There the curtain, tilted at 45° with respect to the horizontal plane, intersects the beams. The gas curtain's path eventually ends at a dump, where it gets evacuated. An extra skimmer blocks gas backscattering from the dump toward the interaction chamber. All chambers are made of 316 LN stainless steel and are equipped with pumping groups and pressure gauges, allowing to keep adequate background pressure levels.

The BGC monitor has been conceived to be installed in the LHC as part of the HEL in the last stage of the project. In the first stage (phase I), a so-called demonstrator, consisting only of the interaction chamber, was installed as part of the LHC beamline (clockwise direction). It was used to perform distributed gas injections during LHC operation in 2022. The following step (phase II) consisted of the installation of the remaining chambers at the LHC to build the complete BGC version 3 (from now on referred to only as *BGC*). This operation was carried out during the year end technical stop (YETS) 22/23. Before phase II,

*cristina.castro.sequeiro@cern.ch

Published by the American Physical Society under the terms of the [Creative Commons Attribution 4.0 International](https://creativecommons.org/licenses/by/4.0/) license. Further distribution of this work must maintain attribution to the author(s) and the published article's title, journal citation, and DOI.

TABLE I. Pump down and injection tests.

Test	Initial conditions		Injections at 5 bar
	Venting gas	Int. chamber	
1	N ₂	Nonisolated	N ₂ (twice)
2.1	Ne	Nonisolated	Ne (several times)
2.2	Ne	Isolated	No injection
3	Air	Isolated	No injection

the BGC equipped with a laboratory interaction chamber has been installed in an off-line laboratory at CERN (from March to October 2022), and as part of the electron beam test stand (EBTS) by November 2022. This allowed for various tests to be carried out [8,9]. The following section describes the vacuum tests performed in the off-line laboratory. Their results have been used to design the vacuum control system and as input for simulations carried out to investigate the BGC behavior and predict the impact of its installation and operation as part of the LHC beam-line. A description of these simulations and their results is given in the second part of this document.

II. OFF-LINE LABORATORY TESTS

Four tests were designed with the aim of characterizing the pump down of the BGC after venting using three different gases and defining its behavior during gas injections. The gases considered for venting were N₂ (99.9999% purity) and

Ne (99.999% purity) (the two working gases) and atmospheric air (to recreate the conditions after the assembly of the remaining chambers into the LHC beamline). The tests start with the chambers at rough vacuum levels. Once they are vented, the pump down begins, and the pressure is recorded. Gas injections were performed during pump down in two out of the four tests. The effect of isolating the interaction chamber from adjacent chambers over the pump down was also studied. Table I summarizes the pump down tests and their conditions.

Figure 1 shows the vacuum layout of the BGC tested in the off-line laboratory. The BGC chambers are provided with different types of pressure gauges and pumping groups composed of a primary pump and a turbomolecular pump. Three gate valves allow the isolation of the interaction chamber from the rest of the chambers and from its own pumping group. Pressure readings can be recorded on a laptop, which also allows for controlling the pumping groups and the gate valves. The injection line is equipped with manual valves to control the gas flow and a primary pump (only attached when used) to remove the gas that accumulates during injections at the nozzle’s volume.

Test results have shown that pressures under 10⁻⁸ mbar have been reached after several hours of pump down in N₂ and Ne venting tests (tests 1, 2.1, and 2.2). Slight differences have been found between the pump down times of the chambers adjacent to the interaction chamber in tests 2.1 and 2.2 (Ne venting, interaction chamber nonisolated and isolated, respectively). These could be explained by the

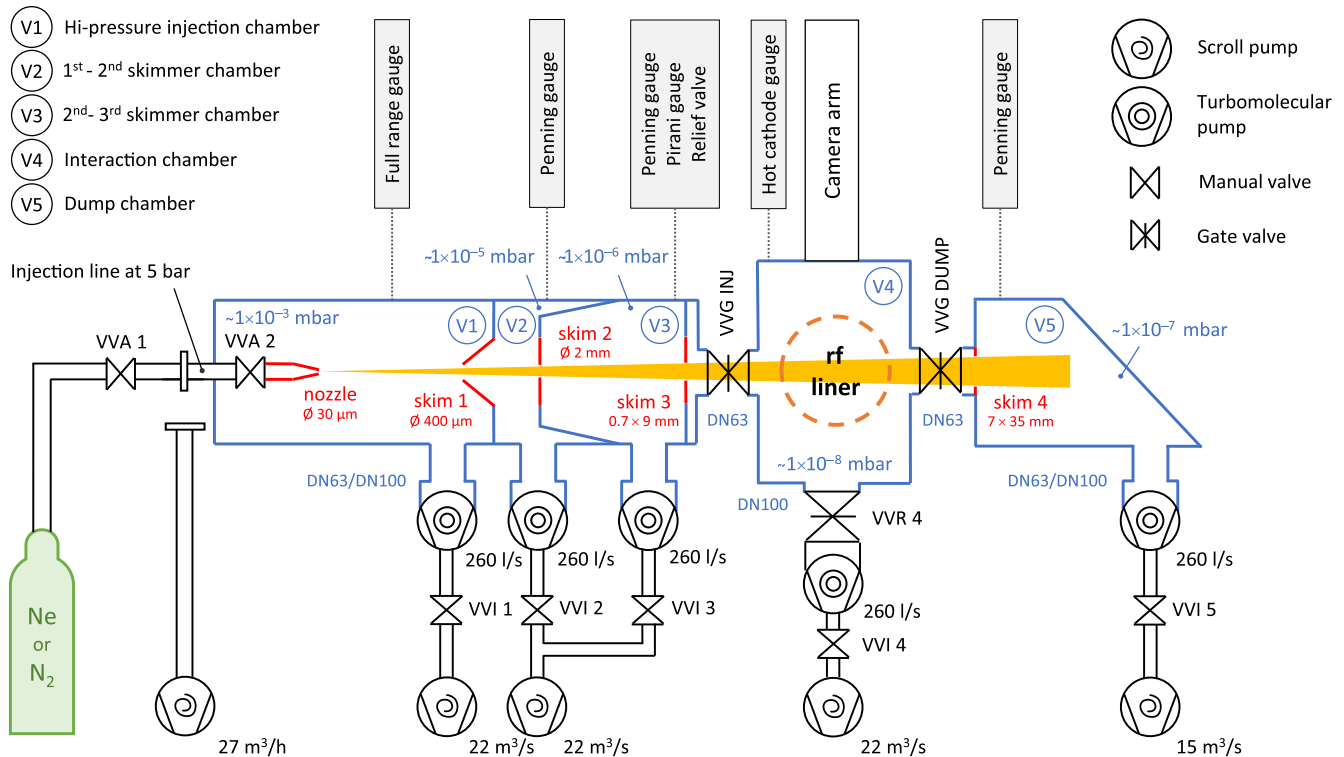


FIG. 1. Vacuum layout of BGC installed in the off-line laboratory.

TABLE II. Increment of pressure due to injections at each chamber. The values shown are averages, except for the interaction chamber, for which measurements were finally made using a Penning gauge instead of the hot cathode gauge. As the gauges provide N_2 equivalent measurements, Ne measurements have been corrected using a factor of 4.1 for Penning gauges and 2 for the full range gauge at pressures above 10^{-3} mbar, following the specifications of the gauges.

	Δ Pressure test 1 (N_2) (mbar)	Δ Pressure test 2.1 (Ne corrected) (mbar)
Hi-pressure injection chamber	5.1×10^{-3}	4.9×10^{-3}
1st–2nd skimmer chamber	1.2×10^{-5}	
2nd–3rd skimmer chamber	1.1×10^{-6}	4.7×10^{-6}
Interaction chamber	5.2×10^{-8}	1.9×10^{-7}
Dump chamber	1.2×10^{-7}	5.4×10^{-7}

fact that the interaction chamber pumps part of the 2nd–3rd skimmer chamber, and in turn, the dump chamber pumps part of the interaction chamber when valves are open. Test 3 (air venting) showed the slowest pump down reaching 10^{-8} mbar after 3 days, as a result of the contamination of the chambers with H_2O , whose desorption rate is generally slower than for other molecules. In tests 2.2 and 3, the pressure recordings allowed the observation of fluctuations due to daily thermal variations.

Regarding the gas injections, in both N_2 and Ne cases (tests 1 and 2.1), the pressure increased quickly inside each chamber after allowing the gas flow to pass. It returned to residual levels after stopping the injection, an action that blocks the injection line and evacuates the gas accumulated at the nozzle. In test 2.1, a pressure peak followed by a smooth decrease was detected in the injection chamber during the multiple Ne injections. This peak could be produced by the presence of air introduced along with the gas. Table II collects the pressure change measured at each chamber during both types of injections.

The information collected in the tests described in this section allowed to carry out the work presented in the following section, being used as input for several simulations. It has also been crucial for the design of the control system to be used in the LHC, defining the threshold values for the safety interlocks.

III. SIMULATIONS AND ANALYTICAL CALCULATIONS

A. H_2O throughput to the LHC from BGC unbaked chambers and NEG coating saturation

During phase II, the remaining BGC chambers were assembled at the interaction chamber already installed

within the LHC beamline. This operation should be followed by the pump down of these chambers, and the opening of the gate valves VVG INJ and VVG DUMP, to connect the added chambers with the LHC beamline. The main vacuum-related concern at this point is whether the residual H_2O still adsorbed on the surface of these chambers can saturate an excessive length of the non-evaporable getter (NEG) coating in the BGC vicinity. If this is the case, the chambers must be baked out in advance.

To determine the impact of H_2O on the NEG coating, first, the quantity of H_2O that would reach the LHC beamline has been calculated using data from test 3 (pump down after air venting with gate valves closed). To do so, the relation between the pressure in the chambers and H_2O outgassing from their surfaces has been obtained using the simulation software Molflow+ [10]. This relation allows an assessment of the outgassing corresponding to the performed pressure measurements.

In the simulation, a simplified geometry of the BGC has been used, which was created from the internal surface of the chambers. Turbomolecular pumps have been defined by their pumping speed for H_2O , 260 l s^{-1} .

Figure 2 shows the obtained outgassing values for each chamber after 1.5, 2, and 3 days of pump down. A reference value is also shown, corresponding to 10 h of pump down, according to [11]. The comparison of the simulation results with this value reveals that the calculated outgassing is higher in most of the chambers while lower in one case. As the walls of each chamber have a different history and geometry, and the location of the gauges and pumps is different, the discrepancy between the results and the reference value has not been further investigated.

The amount of residual gas after each of the three pump down times considered was obtained by integrating a logarithmic function fitted to the simulation results. Considering that all desorbed particles leave the four chambers and enter the LHC beamline, the saturated area of the beamline has been estimated assuming a surface

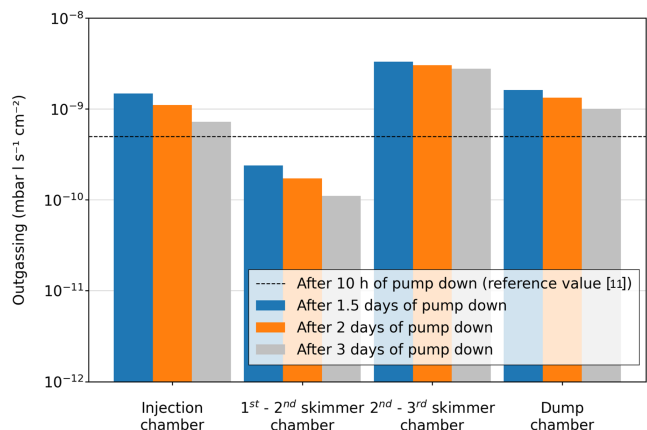


FIG. 2. Outgassing rate at each chamber after different pump down times.

TABLE III. Saturated length of LHC beamline (80 mm diameter) after different pump down times.

Pump down time (days)	Total desorbed particles	Saturated length per side (cm)
1.5	5.4×10^{19}	266
2	4.7×10^{19}	235
3	3.7×10^{19}	182
7	1.1×10^{19}	56

coverage at saturation of 4×10^{15} particles cm^{-2} , since the maximum surface coverage for H_2O is about 5 times larger than for CO (8×10^{14} particles cm^{-2}) [12]. Resulting values are in the order of meters of NEG-coated beamline on both sides of the BGC (Table III). In Table III, an additional case is included, based on the extrapolation of the simulation results for 1 week of pump down. This would reduce the saturated length to 56 cm per side. With these results, it has been considered that the saturation length of the beamline with H_2O can be acceptable provided sufficient pump down time (at least 1 week).

B. Simulation of N_2 and Ne throughput to the LHC beamline from the BGC during operation

Another scenario of interest is the future operation of the BGC within the LHC beamline since working gas molecules will escape the BGC volume and propagate into the beamline. In order to increase the speed of the simulations performed to study this case, the model has been split into two: First, a simulation of the BGC geometry was used to obtain the amount of working gas that leaves the BGC volume; then, a complete model of the BGC and its vicinity allowed for the estimation of the effect the gas molecules would have on the LHC beamline.

In this section, the first model is described, while the LHC simulations are detailed in the following sections.

For the simulation of the BGC, it is necessary to determine the gas entry rate at the injection chamber during 5 bar injections. To do so, an additional simulation of the injections made with the BGC installed in the off-line laboratory has been performed. It allowed for the evaluation of the gas throughput at the 1st skimmer (from where molecular flow conditions can be assumed) by matching the simulated pressure with the laboratory measurements. The pumping speed of the turbomolecular pumps considered for both N_2 and Ne is 260 l s^{-1} . The resulting throughput values are presented in Table IV for both gases.

TABLE IV. N_2 and Ne throughput at the 1st skimmer.

Gas	Throughput at the 1st skimmer (mbar l s^{-1})
N_2	2.4×10^{-2}
Ne	7.6×10^{-2}

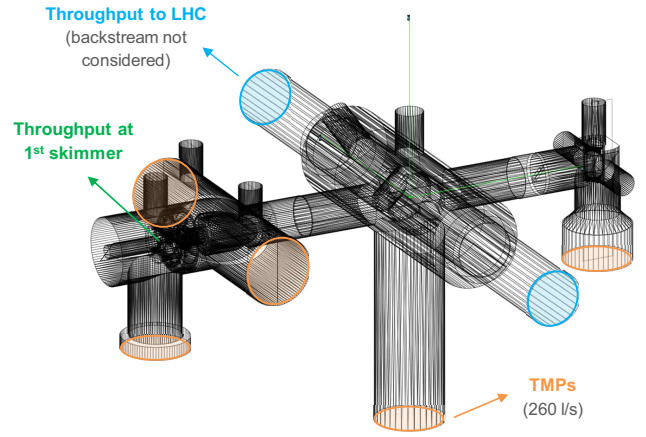


FIG. 3. Inputs for the partial simulation of the BGC installed within the LHC beamline.

Once the gas flow at injection has been obtained, it is used as input for the partial model of the BGC at the LHC beamline (Fig. 3). This model includes two short sections of the LHC beamline 20 cm long. At the ends of these sections, virtual sticking surfaces (marked in blue in Fig. 3) have been defined, representing the pass of particles into the rest of the beamline. Note that this definition of the boundaries of the model does not consider particles that rebound in the LHC beamline and move back to the BGC. These particles have been taken into account in the second, extended model.

In this model, the LHC interaction chamber replaces the one used in the laboratory, while the rest of the BGC geometry remains the same. However, during the tests performed with the monitor at the EBTS, a relevant modification was made to the BGC in view of its installation in the LHC: The 0.7×9 mm 3rd skimmer was replaced by one of smaller size, 0.3×9 mm. Injection tests were performed at the EBTS with both skimmers, allowing for the assessment of the relation between the interaction chamber pressures in the two cases. The pressure with the small skimmer was 0.26 times the pressure with the larger one. This reduction factor has been applied to the BGC operation simulation results in Secs. III C and III D, in which the working gas is Ne , the one finally selected for injections into the LHC beamline since N_2 is discarded (see Secs. III E and V). N_2 results presented in Secs. III E and III F were not downscaled and correspond to the initial large 3rd skimmer geometry.

The rate of particles absorbed by each pump and the throughput values resulting from the partial model simulation are shown in Table V.

C. LHC pressure profile prediction during distributed Ne injections and BGC operation, respectively

The pressure profile resulting along the LHC beamline in the vicinity of the BGC due to Ne injections has been computed for two cases.

TABLE V. Gas exit ratios of BGC installed in the LHC with initial large 3rd skimmer (partial simulation). Row (a) contains the results as the percentage of the throughput at the 1st skimmer, and row (b) as the percentage of the gas that reaches the interaction chamber. Chambers are indicated by the labels in Fig. 1.

	Gas pumped by TMPs				Throughput to LHC (per side)
	V2	V3	V4	V5	
(a)	96.3	3.5	0.01	0.17	0.01
(b)	5.3	84.2	5.3

(i) Distributed gas injections made with the beam gas injection (BGI) system. The injections were performed directly at one port of the interaction chamber (i.e., the demonstrator) installed within the LHC beamline during phase I. Several injections of this type have been executed during 2022 without LHC beam and with different states of the sector valves. Pressure data recorded during these injections have been used to benchmark the simulations. (ii) Injections to be made with complete BGC once installed in the LHC (BGC operation injections). Data obtained from the simulations described in Sec. III B will be used as input in these simulations.

The longest region simulated around BGC (region 1 in Fig. 4) covers up to the cryogenic elements on both sides of the monitor, as they will act as cryopumps stopping the Ne propagation. Upstream, a dipole magnet is installed, which shares the cryostat with an undulator magnet used in the adjacent beamline, and downstream there is an rf module. Between these two cryogenic regions, there is a warm section at room temperature. In this section, there are two beam position monitors and a transverse damper system (ADT). The BGC (or demonstrator) is located next to the dipole magnet, in an independent vacuum sector (region 2).

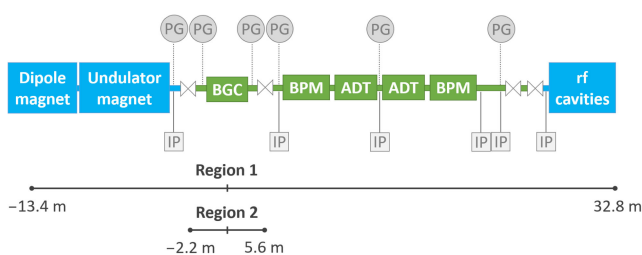


FIG. 4. LHC layout in the vicinity of BGC/demonstrator (left side of LHC point 4). Cryogenic elements are shown in blue, while those in green belong to the warm section. The undulator magnet is located in the adjacent beamline. However, it has been included in the layout as its cryostat houses the BGC's beamline, generating the cryogenic section closest to the BGC. PG and IP indicate the position of a pressure gauge and an ion pump, respectively. The extent of the two regions simulated is also shown.

Regarding the vacuum instrumentation at the LHC, there are six ion pumps and several pressure gauges in this section. During distributed injections, pressure measurements could be obtained from six LHC gauges (indicated in Fig. 4), and also from one gauge placed at the demonstrator during injections with its vacuum sector isolated.

In the simulations, the following inputs have been specified: (i) In each simulation case, the corresponding geometry of the monitor is used: Demonstrator or BGC (Fig. 3). The LHC geometry simulated extends over either region 1 or region 2, and it includes the internal dimensions of the beamline. (ii) The gas flow is set differently for the two cases simulated. For distributed injections, it is defined at the injection port (see Fig. 5) with an arbitrary value as it is an unknown parameter. Pressure results will be later scaled to match the measurements. In the case of BGC operation, the gas flow is defined at two virtual interfaces located in the LHC beamline, in the same position where it was calculated in Sec. III B simulations and with the obtained values. These interfaces are defined in such a way that allows the rebounded molecules to return to the BGC geometry. (iii) In the cryogenic regions, the temperature is defined as 20 K on the beam screen located in the magnets side and 4.5 K in the rf module. It is set at room temperature in the warm section, and in the transitions to cryogenic sections (41.5 cm long on the rf module side and 10.5 cm on the beam screen side), a five-step gradient has been defined. (iv) Regarding the cryogenic pumping, the beam screen at 20 K on the left side does not pump Ne [13]. However, the dipole magnet's cold bore and the drift tube in the undulator section, both surrounding the beam screen, can capture this particle as they are at 1.9 and 4 K, respectively. The particles will be then pumped after passing through the beam screen slots. There is an interconnection between the dipole cold bore and the drift tube, joining the beam screen of both sections, where particles are not

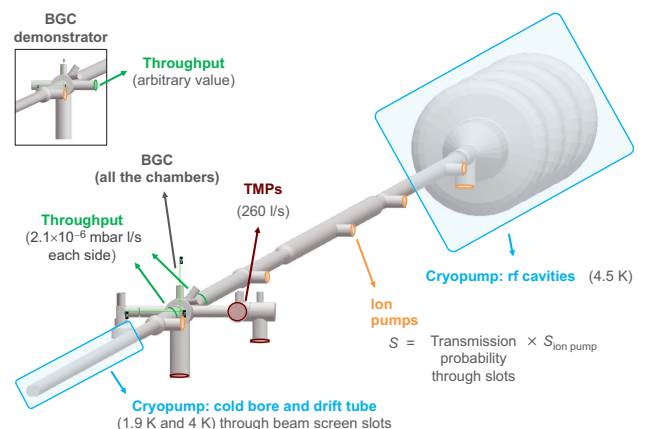


FIG. 5. LHC pressure profile simulation inputs (BGC operation injections with Ne). Detail on the upper left corner shows demonstrator model used in distributed gas injection simulations instead of the complete BGC.

pumped. To simplify the geometry of the model, the pumping speed has been defined at the beam screen surface, where the slots have been replaced by the corresponding transmission probability through them. On the right side, the rf cavities surface, at 4.5 K, will act as a cryopump. (v) As for the ion pumps, their pumping speed varies from 17.5 and 32 ls^{-1} (estimation for Ne). They are attached to different types of modules, in which particles have to cross a surface with slots to reach the pump. The geometry of the modules has been simplified and the surface with slots has been represented by the corresponding transmission probability through them, computed together with pumping speed value at the same location where the pump is defined.

Pressure values (measurements and simulations results) corresponding to distributed injections in region 2 (with sector valves closed) are plotted in Fig. 6. In this case, the pressure was measured in three positions: At the demonstrator and next to the sector valves. The measured data correspond to the pressure increment during three injections at different pressures. The injection pressure, used to define each injection, is the pressure at the BGI injection tube, not at the LHC beamline. The ratio between the injection pressure and the pressure at the demonstrator is between 30 and 50 (higher for higher injection pressures). For comparison, the values of two injections have been scaled to fit the pressure at the demonstrator with the 4.5×10^{-6} mbar injection.

Regarding the simulation results, two alternatives are shown: The results of the model described above (v1), and the results of a model in which a factor of 10 has been applied to the transmission of particles toward the pump.

Model v2 is an attempt to approximate the pressure on the left side to the measured values (the mismatch in this position appeared to be related to a pessimistic

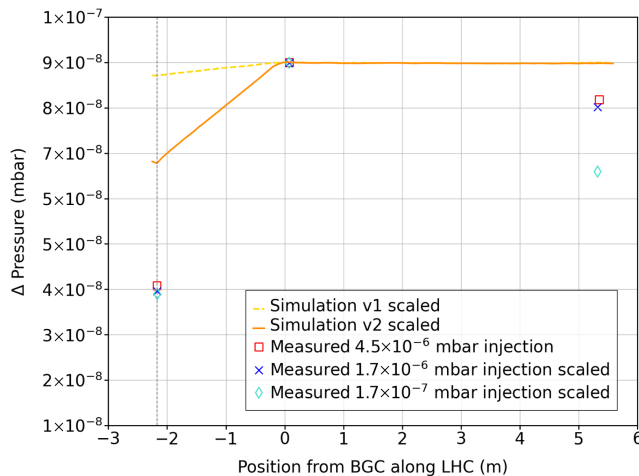


FIG. 6. Pressure profile (simulations and measurements) at the LHC beamline due to Ne distributed injections (pressure increment with respect to the background pressure). Case with sector valves closed (region 2). Dashed line indicates the position of an ion pump. Measured data are Ne corrected.

simplification of the pumps modules). On the right side, the results do not fit either with the measurements, however, it could be expected that they perfectly match: There are no pumps on this side, therefore, the pressure should be the same as in the demonstrator, as the simulations show. No clear reason has been found for this discrepancy. Note that there is some uncertainty in the residual pressure at the LHC (pressure without injection), which affects the pressure increment of injections made at lower pressure to a greater extent, and which also upscales when values are fitted to 4.5×10^{-6} mbar injection.

In Fig. 7, the region 1 case is shown. Measured data have been obtained during distributed gas injections in which the gate valve at the entrance of the cavities was closed. In the same way as in region 2 measurements, the values shown have been scaled for comparison, now to fit the pressure recorded at the second gauge on the right side of the demonstrator with the 4.5×10^{-6} mbar injection. During these injections, the pressure could not be measured at the demonstrator. The ratio between the injection pressure and the average pressure in the four closest gauges to the demonstrator is between 380 and 310 (higher for higher injection pressures).

A first simulation has been carried out in which access to the rf cavities is blocked to compare with the measured data. The assumption made for the transmission of particles

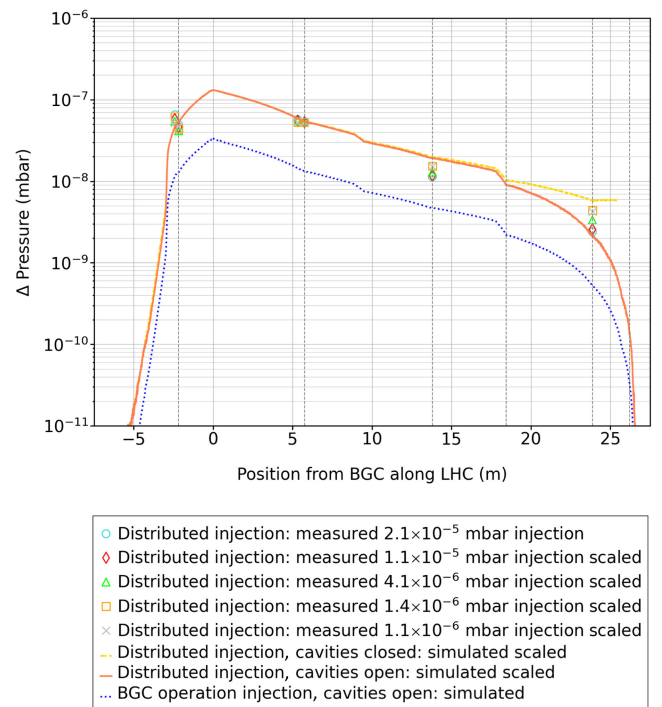


FIG. 7. Pressure profile (simulations and measurements) at the LHC beamline due to Ne injections (pressure increment with respect to the background pressure). Region 1 case. Dashed lines indicate the position of ion pumps. Measured data are Ne corrected.

toward the pumps in region 2 v2 simulation has been applied to region 1 simulations: It has been increased by a factor of 10 in all the ion pumps modules, except for one with a slightly different geometry where a factor of 3 has been used. The plotted results have also been scaled, in the same way as the measurements.

The pressure profile due to BGC operation is also plotted in Fig. 7. The pressure shows the same behavior as in the distributed injections simulations, at the pressure levels corresponding to a 5 bar injection on the BGC injection chamber using the small 3rd skimmer (results, obtained for the large 3rd skimmer, have been downscaled by a factor of 0.26).

D. Gas exit ratios and Ne deposition on cryogenic surfaces during BGC operation

Using the simulation of the BGC operation, the rate of pumped gas at the LHC, at the interaction chamber, and dump chamber has been obtained. These results are shown in Fig. 8. Around the 98% of the gas that reaches the interaction chamber from the 2nd–3rd skimmer chamber is pumped by the turbomolecular pumps at the dump and interaction chambers (85% and 13%, respectively). The remaining $\approx 2\%$ is pumped at the LHC (1.4% at the beam screen—and, thus, deposited at the cold bore and drift tube—and 0.04% at the cavities). The ratios of pumped particles are also indicated as percentage of the gas that reaches the LHC from the BGC. Using this reference, the gas pumped at the LHC is 16.4%, while most of the gas returns to the BGC, pumped mainly by the turbomolecular at the interaction chamber (72%).

Ne particles pumped at the cryogenic regions remain adsorbed to the surfaces. The accumulation of particles in the surfaces around the beam path affects the electron-induced secondary electron emission, which could lead to an exponential mechanism of electron cloud buildup.

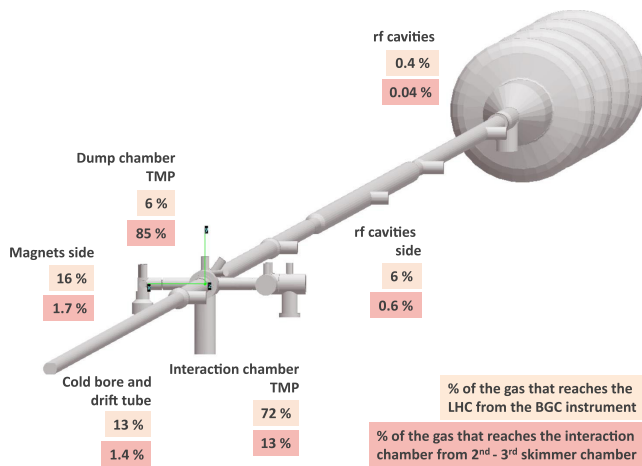


FIG. 8. Ratios of pumped gas at LHC and at interaction and dump chambers.

The electron cloud can have a negative effect in the performance of the LHC, so its buildup has to be minimized [14]. In order to analyze the Ne particles' contribution to the secondary electron yield (SEY), the quantity of gas deposited along the cryogenic elements has been obtained (Figs. 9 and 10). In the graphs on top, values are given per unit of area at every 1 cm section, to compare both cryogenic regions. The second y axis indicates the surface accumulation after 1 day in terms of the number of monolayers, using the relation 1 monolayer equal to 1×10^{15} particles cm^{-2} . In the graphs below, the total quantity of accumulated particles in every section after 1 day is shown. The greatest accumulation occurs at the drift tube closest side to the BGC, where 4.7 monolayers are accumulated after 1 day of continuous injection. At the cold bore, the maximum value is 0.077 monolayers day^{-1} , and at the cavities, it is 0.016 monolayers day^{-1} at their entrance. Taking as reference the accumulated BGC operation time during 2022, around 100 h, the maximum deposition values are 19.6, 0.32, and 0.07 monolayers at the drift tube, the cold bore, and the cavities, respectively. Looking at the SEY variation with primary electrons energy (200 eV for the LHC [14]) for Ne monolayers condensed on a copper substrate [15], the SEY contribution of 28 monolayers is around 0.8. Assuming a linear dependence with the number of monolayers (from Fig. 3 of [15]), the SEY increment after 100 h of continuous operation of the BGC would be 0.56 at the drift tube, 9.1×10^{-3} at the cold bore, and 1.9×10^{-3} at the rf cavities. As a reference, the SEY values measured on Nb surfaces range between 1.1 for baked surfaces and 1.7 for unbaked [16]. Therefore, it can be considered that Ne accumulation on the cold bore and the rf cavities represents

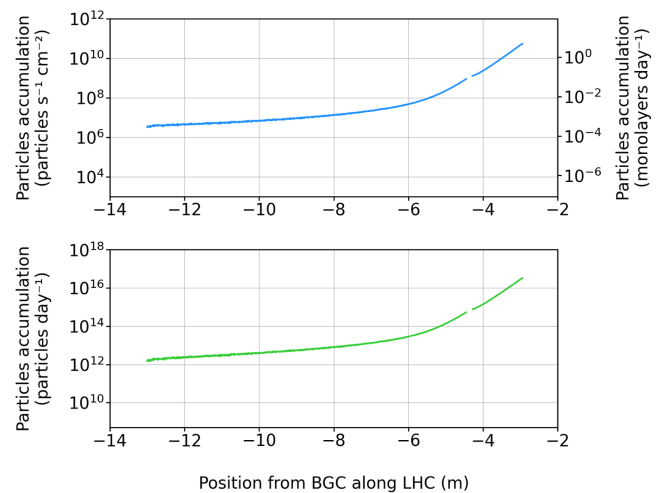


FIG. 9. Ne deposition on the magnets side. The discontinuity in the data corresponds to the location of the interconnection between the dipole magnet's cold bore (on its left) and the drift tube (on its right).

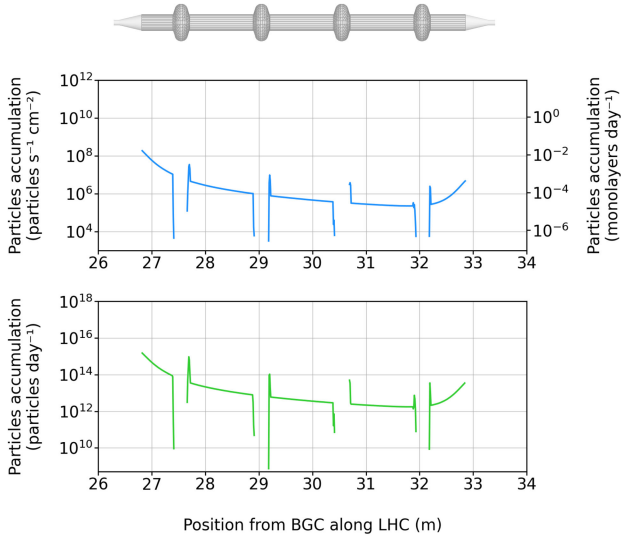


FIG. 10. Ne deposition on rf cavities. On top, geometry corresponding to the plotted section.

a negligible increment on the SEY, whereas it could imply a higher contribution at the drift tube.

E. NEG coating saturation with N₂ during BGC operation and gas exit ratios

In the case of N₂ injections, NEG coating of the LHC beamline must be taken into account in the simulations, as it is capable of absorbing these molecules. The simulation of this case will allow to obtain the NEG coating saturation length and validate the use of N₂ for injections in the LHC. Figure 11 shows the inputs for this simulation. The model covers the region 2, up to the sector valves placed on both sides of BGC so that it includes the two first NEG-coated sections.

Since the sticking factor of the NEG coating varies as it adsorbs particles, iterative simulations are needed to update its value. *VacuumCOST* [17], a Python code which allows to perform such iterative *Molflow+* simulations, has been used for this case.

Due to that lack of information about the surface roughness of the coated beamline, two different cases have been simulated: A beamline coated with a Ti-Zr-V thin film deposited on a smooth copper substrate and on a rough substrate.¹ In the first case, the sticking variation with the surface coverage is faster than in the second one. The data used in the simulations correspond to sticking models obtained from fitting experimental data [18]. The initial sticking is 0.04 (smooth surface) and 0.07 (rough surface). The surface is considered saturated when a coverage of 0.7×10^{14} N₂ particles cm⁻² has been reached in the

¹ $R_a = 0.16 \mu\text{m}$ and $R_t = 1.46 \mu\text{m}$ in the smooth substrate, and $R_a = 0.53 \mu\text{m}$ and $R_t = 4.48 \mu\text{m}$ in the rough case [18].

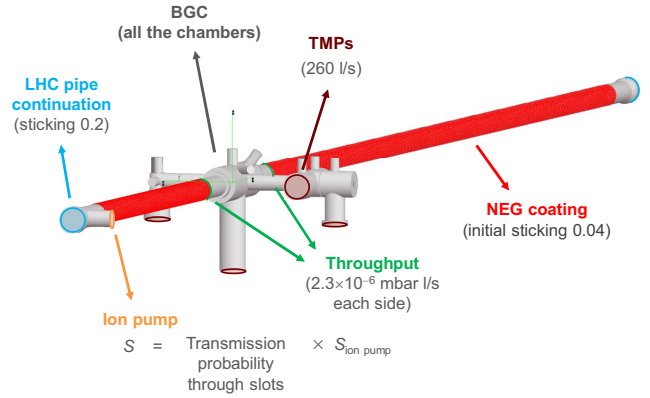


FIG. 11. LHC pressure profile simulation inputs (BGC operation with N₂).

smooth case, and 4.5×10^{14} N₂ particles cm⁻² in the rough case, being the sticking factor of 0.004 in both cases. The sticking factor is applied to small surfaces (of around 1 cm²) in which the NEG-coated surface has been split.

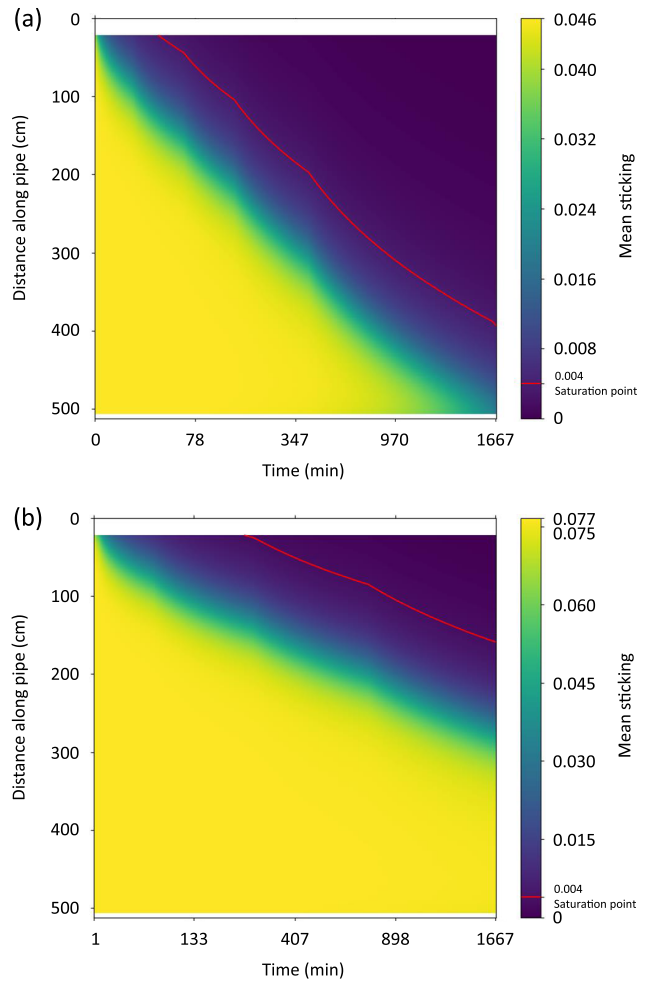


FIG. 12. NEG coating sticking evolution with the time along the BGC downstream beamline. (a) Smooth surface and (b) rough surface.

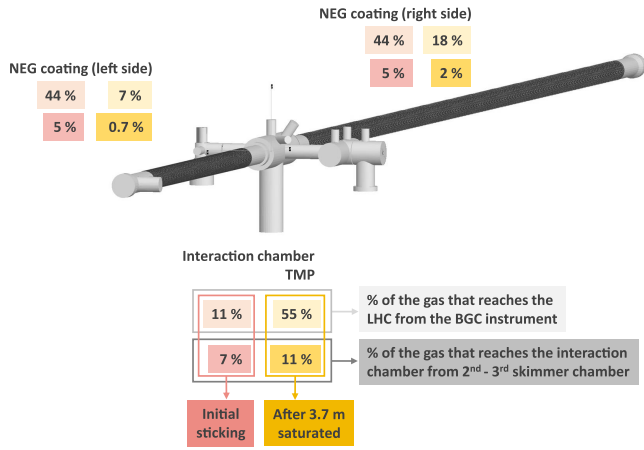


FIG. 13. Ratios of pumped gas at LHC and at interaction and dump chambers. Smooth surface case.

The connection of the LHC beamline at its ends with the rest of the beamline is represented by a sticking factor of 0.2. The gas throughput has been replaced by the value corresponding to N₂, obtained in Sec. III B.

Figure 12 shows in detail the evolution of the sticking factor on the BGC downstream beamline, in both smooth and rough surface cases. In these plots, it can be seen the propagation of the saturation along the length of the beamline with the time, reaching 3.7 m after 27.8 h in the smooth case. With a rough coating, the saturated length is reduced up to 1.4 m after the same time. In both cases, a considerable saturated length is reached in the time considered, and it would be even higher after the reference taken of a total operation time of 100 h.

The resulting pumping ratios for the NEG coating and the turbomolecular placed at the interaction chamber are indicated in Fig. 13 for the smooth case (worst case).

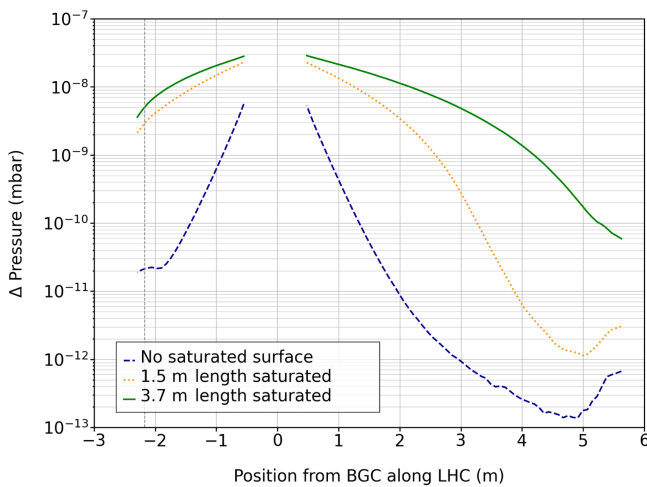


FIG. 14. Pressure profile at the LHC beamline due to N₂ injections at different saturated beamline lengths. Smooth surface case. Data are shown from the two outgassing points.

They have been calculated at two instants: At the beginning of the simulations, when the sticking factor is almost the initial in the beamline; and after 27.8 h, when most of the beamline coating has been saturated. In the first case, most of the gas is adsorbed on the NEG coating; in the second, the turbomolecular pumps the greater part. Values are shown as percentage of the gas that reaches the interaction chamber from the 2nd–3rd skimmer chamber, and of the gas that reaches the LHC from the BGC.

F. LHC pressure profile prediction during N₂ injections (BGC operation)

The pressure profile has been obtained at three different instants of the smooth surface simulation described in the previous section (Fig. 14). Each case corresponds to a determined saturated length of the NEG-coated beamline: No saturation at the beginning, 1.5 m on both sides of BGC, and 3.7 m after 27.8 h.

IV. INSTALLATION AND OPERATION

Phase II has been completed during YETS 22/23. The BGC (including its control system) has been successfully installed and commissioned and is currently operating using Ne gas. It has proved to be an LHC vacuum-compatible system, and no adverse effects have been detected on the elements in the vicinity of the BGC. The functionality of the monitor has been verified achieving the first measurements of the LHC proton and Pb beams, at both beam injection and flattop energies (450 GeV and 6.8 TeV, respectively). These measurements are out of the scope of this document and will be presented in separate publications.

V. CONCLUSIONS

A series of tests were performed in the off-line laboratory with the BGC before its installation in the LHC. The pump down after venting with N₂, Ne, and atmospheric air was characterized, with the last case presenting the slowest pump down. Pressure measurements during N₂ and Ne injections were also carried out during these tests.

The results obtained in the tests contributed to the LHC control system design, providing values for the pressure safety interlocks and helping to choose the final instrumentation to be installed in the LHC.

The collected data were also used as input in the various studies carried out to estimate the impact of the BGC on the LHC beamline, presented in this document.

In these studies, the saturation of the beamline NEG coating in the vicinity of the BGC with H₂O desorbed from the unbaked chambers has been estimated. Based on the results, an acceptable compromise between time spent on pumping and the resulting saturated length has been found, which made it possible to dispense with bakeout.

LHC simulation models have been developed for the BGC vicinity, allowing to obtain the Ne and N₂ pressure profiles during BGC operation along the LHC beamline.

The Ne deposition on cryogenic surfaces has also been simulated, with the results indicating a low impact in the SEY at the dipole magnet's cold bore and the rf cavities, but higher in the cryogenic drift tube located between the dipole magnet and the BGC, case that should be subject of further studies.

In the case of N₂, the analysis of the NEG coating saturation during BGC injections led to it being considered unsuitable for its use at the LHC.

-
- [1] S. Redaelli, R. B. Appleby, R. Bruce, O. Brüning, A. Kolehmainen, G. Ferlin, A. Foussat, M. Giovannozzi, P. Hermes, D. Mirarchi *et al.*, Hollow electron lenses for beam collimation at the High-Luminosity Large Hadron Collider (HL-LHC), *J. Instrum.* **16**, P03042.
- [2] V. Tzoganis and C. P. Welsch, A noninvasive beam profile monitor for charged particle beams, *Appl. Phys. Lett.* **104**, 204104 (2014).
- [3] A. Salehilashkajani, H. D. Zhang, M. Ady, N. Chritin, P. Forck, J. Glutting, O. R. Jones, R. Kersevan, N. Kumar, T. Lefevre *et al.*, A gas curtain beam profile monitor using beam induced fluorescence for high intensity charged particle beams, *Appl. Phys. Lett.* **120**, 174101 (2022).
- [4] V. Tzoganis, H. D. Zhang, A. Jeff, and C. P. Welsch, Design and first operation of a supersonic gas jet based beam profile monitor, *Phys. Rev. Accel. Beams* **20**, 062801 (2017).
- [5] J. Kamiya, N. Ogiwara, A. Miura, M. Kinsho, and Y. Hikichi, Nondestructive 2-D beam profile monitor using gas sheet in J-PARC LINAC, *J. Phys. Conf. Ser.* **1067**, 072006 (2018).
- [6] Y. Hashimoto, T. Fujisawa, T. Morimoto, Y. Fujita, T. Honma, S. Muto, K. Noda, Y. Sato, and S. Yamada, Oxygen gas-sheet beam profile monitor for the synchrotron and storage ring, *Nucl. Instrum. Methods Phys. Res., Sect. A* **527**, 289 (2004).
- [7] F. Favela, L. Acosta, E. Andrade, V. Araujo, A. Huerta, O. G. de Lucio, G. Murillo, M. E. Ortiz, R. Policrioniades, P. Santa Rita *et al.*, New supersonic gas jet target for low energy nuclear reaction studies, *Phys. Rev. ST Accel. Beams* **18**, 123502 (2015).
- [8] R. Veness, M. Ady, C. Castro Sequeiro, P. Forck, N. Kumar, T. Lefevre, S. Mazzoni, I. Papazoglou, A. Rossi, A. Salehilashkajani *et al.*, Design of a prototype gas jet profile monitor for installation into the Large Hadron Collider at CERN, in *Proceedings of the 13th International Particle Accelerator Conference, IPAC-2022, Bangkok, Thailand* (JACoW, Geneva, Switzerland, 2022), pp. 363–366, [10.18429/JACoW-IPAC2022-MOPOPT048](https://doi.org/10.18429/JACoW-IPAC2022-MOPOPT048).
- [9] H. D. Zhang, N. Kumar, A. Salehilashkajani, O. Sedlacek, O. Stringer, C. P. Welsch, M. Ady, T. Lefevre, S. Mazzoni, I. Papazoglou *et al.*, Commissioning of a gas jet beam profile monitor for EBTS and LHC, in *Proceedings of the 13th International Particle Accelerator Conference, IPAC-2022, Bangkok, Thailand* (JACoW, Geneva, Switzerland, 2022), pp. 393–396, [10.18429/JACoW-IPAC2022-MOPOPT056](https://doi.org/10.18429/JACoW-IPAC2022-MOPOPT056).
- [10] R. Kersevan and M. Ady, Recent developments of Monte-Carlo codes Molflow+ and Synrad+, in *Proceedings of the 10th International Particle Accelerator Conference, IPAC-2019, Melbourne, Australia* (JACoW, Geneva, Switzerland, 2019), pp. 1327–1330, [10.18429/JACoW-IPAC2019-TUPMP037](https://doi.org/10.18429/JACoW-IPAC2019-TUPMP037).
- [11] P. Chiggiato, Outgassing properties of vacuum materials for particle accelerators, in *Proceedings of the 2017 CERN Accelerator School Course on Vacuum for Particle Accelerators, Glumslöv, Sweden* (CERN, Geneva, Switzerland, 2017), p. 143 [arXiv:2006.07124].
- [12] P. Chiggiato and P. Costa Pinto, Ti–Zr–V nonevaporable getter films: From development to large scale production for the Large Hadron Collider, *Thin Solid Films* **515**, 382 (2006).
- [13] V. Baglin, Cryopumping and vacuum systems, in *Proceedings of the 2017 CERN Accelerator School Course on Vacuum for Particle Accelerators, Glumslöv, Sweden* (CERN, Geneva, Switzerland, 2017), p. 257 [arXiv:2006.01574].
- [14] F. Zimmermann, Electron-cloud effects in the LHC, in *Proceedings of the Mini Workshop on Electron Cloud Simulations for Proton and Positron Beams, Geneva, Switzerland* (CERN, Geneva, Switzerland, 2002), p. 57, [10.5170/CERN-2002-001](https://doi.org/10.5170/CERN-2002-001).
- [15] J. Cazaux, Y. Bozhko, and N. Hilleret, Electron-induced secondary electron emission yield from condensed rare gases: Ne, Ar, Kr, and Xe, *Phys. Rev. B* **71**, 035419 (2005).
- [16] N. Hilleret, C. Scheuerlein, and M. Taborelli, The secondary-electron yield of air-exposed metal surfaces, *Appl. Phys. A* **76**, 1085 (2003).
- [17] P. L. Henriksen, M. Ady, and R. Kersevan, Vacuum chamber conditioning and saturation simulation tool (VacuumCOST): Enabling time-dependent simulations of pressure and NEG sticking in UHV chambers, *Vacuum* **212**, 111992 (2023).
- [18] A. Prodromides, Nonevaporable getter thin film coatings for vacuum applications, PhD thesis, Ecole Polytechnique Federale de Lausanne, 2002.